UCRL- 88257
PREPRINT

UCRL--88257

DE83 014961

CYTOMETRIC ANALYSIS OF MAMMALIAN SPERM FOR INDUCED MORPHOLOGIC AND DNA CONTENT ERRORS

Daniel Pinkel

BIOMEDICAL SCIENCES DIVISION

This paper was prepared for submittal to
Proceedings of the International Symposium on
Biological Dosimetry:
Cytometric Approaches to Mammalian Systems

June 27, 1983

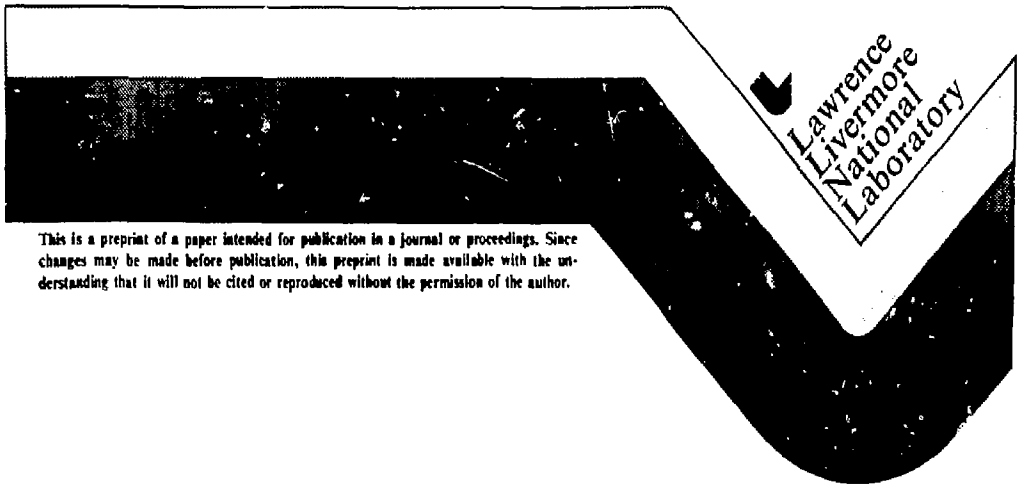

CYTOMETRIC ANALYSIS OF MAMMALIAN SPERM FOR INDUCED MORPHOLOGIC AND DNA CONTENT ERRORS

Daniel Pinkel

Lawrence Livermore National Laboratory

Biomedical Sciences Division

University of California

P.O. Box 5507 L-452

Livermore, California 94550

Work performed under the auspices of the U.S. Department of Energy by the Lawrence Livermore National Laboratory under contract number W-7405-ENG-48.

2506B*/133B

TABLE OF CONTENTS

1. INTRODUCTION

Among the signatures of reproductive toxicity of chemical and physical agents are alterations in morphology and/or DNA content of sperm. Sperm based assays for reproductive effects are attractive because of the potential for obtaining samples for monitoring human populations. Visual analysis of sperm morphology has been used for many years as one component of semen assessment. More recently it has been found that shape abnormalities are induced by exposure of animals to a wide range of agents (27,28) and there is evidence for elevated levels of abnormally shaped sperm in men exposed to drugs or chemical agents in the work place (29). Experienced observers are consistent in classifying sperm according to shape but classification criteria may differ among them. Additionally there are important aspects of sperm shape which humans can't discriminate well. These considerations have led to efforts to develop quantitative morphologic analysis procedures. These procedures lend themselves to automation, so that once their value is established the time required for large numbers of analyses may be greatly reduced.

DNA content errors in germ cells have been detected by cytological techniques (12,21,22) at specific points during spermatogenesis such as meiosis, and the consequences of the errors have been determined by post fertilization karyotype analysis (3,4,6,7,12,14). Recently flow cytometric measurements have been able to detect radiation induced DNA content errors in sperm (19) and spermatids (10,11), yielding information where it was previously unavailable.

In this article I will review some flow-cytometric and image analysis procedures under development for quantitative analysis of sperm morphology. I will also summarize the results of flow-cytometric DNA-content measuremen

sperm from radiation exposed mice, relate these results to the available cytological information, and discuss their potential dosimetric sensitivity.

2. SPERM HEAD MORPHOLOGY

Mammalian sperm have thin planar heads attached to a long tail. Morphologic abnormalities may occur in both. Procedures for quantitatively classifying sperm shape range from simple measurements of head length (13) to complex dexcriptions of both head and tail (28). To illustrate the possibilities and problems of this work I will summarize two image analysis and one flow cytometric study of changes in mouse sperm head shape induced by x-ray exposure.

2.1 Image-Analysis Studies

Quantitative assessment of changes in sperm head shape due to toxic exposure requires establishing of a set of measurements of cell features which are sensitive to the changes. Parallel experiments by Moore et al. (16) (called MBKW in what follows) and Young et al. (30) (called YGLW) illustrate two methods of approaching this problem. Both studies analyzed sperm from the same mice, which had been exposed to testicular x-ray doses of 0, 30, 60, 90, and 120 rad. The three mice in each dose group were killed 5 weeks after exposure and smears of sperm from the cauda epidydimides were prepared. MBKW stained the smears with the protein stain eosin which allowed visualization of the whole sperm head. YGLW used the DNA stain gallocyanin chrome alum which stained the nucleus. Since the sperm head is almost entirely nucleus the visible sperm shapes were basically the same in these two studies. Five hundred eosin stained sperm from each mouse were visually classified as normal or abnormal (5) so that the image analysis results could be compared with a

dose-response curve generated by an experienced human observer. MBKW took photomicrographs (8500x) of 50 randomly selected sperm per mouse and manually measured 9 linear features believed to describe sperm head shape (Fig. 1) as well as area, perimeter, and perimeter^2/area. YGLW used a microscope-based, computer image-analysis system in which the outlines of the sperm nuclei were defined using a thresholding technique (Fig. 2). They then computed 10 general descriptions of cell shape. These included area, perimeter, perimeter^2/area, and 7 others describing the curvature, roughness, and deviation from circularity of the sperm nuclear outline. No measurements of linear or diagonal dimensions were included. Thus only 3 of the measured features in the two studies were the same.

Visual scoring of sperm heads is based on classifying each as normal or abnormal, and perhaps recognizing several different classes of abnormalities. Quantitative measurements allow the establishment of rigorous criteria for this classification and also make it possible to study changes in each dose group as a whole. The simplest way to describe a group is with the average values and variances for the measured features. The results obtained in the two studies were different. MBKW found no significant changes in the means of their measurements, but did find an increase in the variances in the highest dose groups. On the other hand, YGLW found changes in the mean values of some features but did not report changes in the variances. In the three features measured in common, there is disagreement on their behavior.

Sensitivity was greatly improved in both studies by combining individual measurements into a statistical measure called the Mahalonobis distance, M. This describes the "distance" in the multidimensional feature space by which a cell or experimental population departs from a reference population. The

distance is measured in units related to the variance and covariance of the measurements in the reference population. Explicitly,

$$M = (Y - \bar{Y}_c)' S^{-1} (Y - \bar{Y}_c) \qquad (1)$$

where Y is a vector whose elements are the measured features on a particular cell, $\bar{Y}_c$ is the mean value of the feature vector, for the reference population (the ' indicates the transpose of the vector) and S^{-1} is the inverse of the covariance matrix for the reference population (YGLW calculated S^{-1} by pooling both the exposed and reference populations).

MBKW applied Eq. (1) to each sperm head in each dose group using the zero dose sperm for the reference population. They found that the mean M for each dose group increased with dose but that more sensitivity could be achieved by classifying each sperm as normal or abnormal based on its M value. This was done by defining those with M larger than some critical value as abnormal. Figure 3 shows a series of dose-response curves obtained in this way. A choice of ~ 45 for the critical value approximately duplicates the visually obtained dose-response curve. Choosing lower values yields steeper slopes at the expense of classifying more sperm in the unexposed group as abnormal.

The dose-response curves of Fig. 3 were based on all 11 features. MBKW then searched all possible subsets of combinations of 1, 2, ... etc. features to see which yielded the greatest sensitivity to exposure. Searches of this type have to be carried out by directly testing all of the possible combinations, in this case 2047. The search was constrained in two ways. First the critical value of M was chosen such that at zero dose 3% of the

sperm were classified as abnormal, in agreement with the visual scoring. Second, the resulting dose-response curve was required to be well fitted by a straight line. These subsets were then compared on the basis of the slopes of their dose-response curves. It was found that several subsets yielded greater slopes than the complete set of all 11 features. Thus "noise" in some of the features was obscuring response in the others. The features L_2, L_4, D_2, and area (Fig. 1) appeared in most of the high-slope subsets and thus appear to be more sensitive to radiation exposure than the others. The doubling dose (the dose required to double the percentage of abnormal sperm in the control group) for these subsets was less than 25 rad compared to about 70 rad for visual scoring. Sperm-by-sperm comparisons of visual and quantitative classification indicate that the additional sensitivity of the latter comes from changes in the area and diagonal measurements, quantities not easily judged by eye.

YGLW applied Eq. (1) to the sperm populations as a whole, using the mean values of the features of the sperm from each mouse and thus calculating a single M for the sperm from that animal. No classification of individual sperm as normal or abnormal was reported. The resulting dose response curve was fitted by an equation of the form $M = a D^b + c$, where M is the Mahalonobis distance at dose D, c is the zero dose intercept, a is a constant, and $3 < b < 4$.

Several issues raised by these studies remain unresolved. Application of the calculation of YGLW to the measurements of MBKW would have found essentially no response to dose since the means of their measured features were very nearly dose-independent. MBKW found it most sensitive to classify individual sperm based on their M value and searched for and found

dose-response curves that were well fitted by a straight line. YGLW found a cubic or quadratic behavior of M for the groups and reported no attempt to classify individual sperm. Experience with visual scoring has found dose-response curves increasing approximately as $D^{1.5}$ where D is the dose. The differences in the shape of the curves may be related to the different information captured by the measured features in each case. This issue is important since the sensitivity of the assay at low doses depends on the slope of the curve at D = 0; the larger the exponent the larger the dose required to measure a response.

Methodological improvements might also resolve some of the differences between the quantitative studies. It is important to establish the sampling density required to adequately describe sperm head shape in digital images. It is also important that automatic procedures for finding the sperm head outline be carefully monitored to be sure that the acquired image is that of a single sperm lying flat on the slide and that the computer-found perimeter not contain artifactual deviations due to debris near the cell being measured. This is especially important in rodent sperm because their hooked shape (Fig. 1) results in a normal outline with regions of high curvature. While these studies point up issues that require resolution, they indicate the potential of quantitative sperm head measurements to improve the sensitivity and objectivity of morphological classification. They allow a rigorous definition of classification criteria and the testing for those features most affected by exposure to toxic agents.

2.2 Flow Cytometry

Slit-scan flow cytometry has been used to obtain one-dimensional morphological information about cells and chromosomes. Benaron et al. (2)

have applied it to the detection of x ray induced sperm head shape abnormalities. In their work sperm whose nuclei were stained with a fluorescent DNA specific dye were scanned as they flowed through an elliptically focused laser beam whose dimension along the direction of flow (2.5 μm) was much less than the length (~7 μm) of the nucleus (Fig. 4). The hydrodynamic forces associated with the flow oriented the sperm so that they flowed either head or tail first through the beam. Because of the optical effects peculiar to sperm (see Section 3) data were only accepted from sperm which were oriented such that their plane was approximately normal to the axis of the fluorescence collection lens. This was judged by the brightness of the integrated fluorescence signal (cells in the peak of Fig. 6a). Fluorescence intensity was recorded every 20 ns so that about 50 measurements defined the profile of the fluorescence pulse. The information contained in the pulse profile is the DNA content in a series of strips across the cell. Its relation to cell shape as seen by a human observer and the image analysis techniques discussed above is indirect. For example, the slit scan signal is sensitive to thickness variations in the nucleus which were not determined in the other studies (but could have been).

A sperm head was classified as normal or abnormal by comparing the shape of its fluorescence profile, the sequence of 50 or so individual measurements $\{a(i)\}$, with a standard profile $\{b(i)\}$ obtained by averaging the profiles of 100 sperm from a control population. The departure from standard was quantified by the sum of the squares of the differences (SSD) of the two sets of numbers

$$SSD = \Sigma_i [a(i) - b(i)]^2. \qquad (2)$$

Sperm with an SSD value above a chosen threshold were defined as being different from the standard.

A comparison of the flow and visual scoring of sperm from mice exposed to testicular radiation doses between 0 and 900 rad is shown in Fig. 5. The curve depends on the choice of SSD threshold and the one shown corresponds to the value that gives highest correlation with visual scoring. The difference in the background rates of sperm classified as abnormal may be due to a number of factors such as inadequate control of cell orientation during measurement or to actual shape variability, such as nuclear thickness, to which visual observers are not sensitive. Further work is needed to define these factors and perhaps to develop other methods of processing the profiles to define morphological differences. For example, small differences in the length of a sperm nucleus are weighted heavily in the SSD calculation because of the steepness of the fluorescence profile at the ends of the sperm head (Fig. 4). While the information contained in the flow profiles is less complete than that used for visual and quantitative image analysis, the potential for high analysis rates inherent in flow cytometry may compensate for the poorer resolution. Slit scanning may also capture aspects of sperm shape variability missed by other techniques.

3. DNA CONTENT

The incidence of sperm with abnormal DNA content increases after exposure of males to various chemical and physical agents. Two general classes of abnormalities have been of interest. The first consists of polyploid sperm, the most prevalent of which are diploid. The second includes errors of much smaller magnitude such as chromosomal translocations or abnormal chromosome

number due to nondisjunction. The size spectrum of the latter results in variability of the DNA content in the sperm population. Diploid sperm occur in mammals with frequencies on the order of 10^{-3} to 10^{-4} and in special cases as high as 10^{-2} (1,9). Diploid sperm incidence has been shown to be elevated by exposure of animals to radiation and certain chemicals (23,25). Manual scoring of such an assay is laborious because of the low frequency of occurrence. In section 3.1 I will describe one application of flow cytometry to determine the incidence of diploid mouse sperm as a function of x-ray dose.

The smaller DNA content errors can be detected during spermatogenesis by examination of the condensed chromosomes at the cell divisions (12,21,22). Karyotype analysis after *in vitro* or *in vivo* fertilization can be used to determine the incidence of sperm with chromosomal abnormalities which complete spermatogenesis and are capable of fertilization (3,4,6,7,12,14). In special cases particular chromosomes can be visualized in spermatids and sperm by exploiting their unique staining properties and so that errors in their freequency may be recognized (23,24). Flow-cytometric techniques capable of measuring DNA content of sperm and spermatids with sufficient accuracy to detect these errors have recently been developed (15,20). In sections 3.2 and 3.3 I will discuss these measurements, compare the information obtained from them with that obtained from cytologic techniques, and finally speculate on the sensitivity of flow measurements in animals other than the mouse. Measurements of induced DNA content variability in mouse spermatids is discussed by U. Hacker elsewhere in this volume (10) and in Ref. 11.

3.1 Diploid Sperm

Flow-cytometric detection of diploid sperm requires discrimination of true diploid cells from doublets of normal sperm, whose frequency is difficult to

reduce below 1%. Our approach has been to index sort suspected diploid sperm and confirm their status by quantitative microscopic examination. These measurements, which are still preliminary, were made on sperm from mice collected 35 days after local testicular x-ray exposure. Sperm were stained with the acriflavine-Feulgen technique (20) and each object with a diploid fluorescence intensity was single-drop index sorted in a rectangular array on an agarose coated microscope slide. The stain stayed in the cell after the drop dried. Since the sorter was not equipped to fully compensate for the optical problems of sperm measurement (Fig. 6) the sort windows were chosen to cover the wide range of expected diploid intensities. Each drop was then examined on a quantitative fluorescence microscope. If a drop contained a single sperm that cell was a candidate for being diploid. Its fluorescence intensity was then measured for confirmation. A preliminary dose response curve is shown in Fig. 7. Since the error bars can be reduced by counting more cells, these measurements can be made very precise. At high doses there is a several order of magnitude increase in the incidence of diploid mouse sperm, roughly in agreement with the spermatid data of Tates (23,25), but at low doses the response is very flat. Because of the limited number of measurements performed so far, it is not certain this apparent threshold behavior is correct. Confirmation of this dose response relation requires more measurements.

3.2 Sperm DNA Content Variability

Flow-cytometric DNA content measurements of sperm are complicated by the highly condensed state of the nucleus (26). This makes accurate fluorescent staining for DNA difficult and results in a high index of refraction. The index of refraction coupled with the flatness of the cell makes fluorescence

measurements sensitive to the orientation of the cell with respect to the excitation beam and the detectors (Fig. 6a). Thus special staining and optical techniques are required for accurate measurement (20). Two techniques have demonstrated the capability to overcome the optical problems. One hydrodynamically orients the sperm heads (Fig. 6b), and the other, for example the commercially available ICP 22 flow cytometer (Ortho Instruments) measures the cells while they are flowing along the optical axis (Fig. 6c). To solve the staining problems, proteolytic decondensation of the nucleus is usually employed. With these techniques the X and Y sperm populations of many species can be clearly resolved (8) and in one case separated (18). While this resolution is occasionally achieved with human sperm (17) it is very infrequent presumably because the chromatin of human sperm is less uniformly condensed than that of other species.

A flow-cytometrically obtained dose-response curve describing the increase in DNA content variability, CV_D^2, as a function of x-ray dose for mouse sperm is shown in Figure 8 (19). CV_D^2 is the dose-dependent component of the square of the coefficient of variation of the sperm fluorescence frequency distributions. For this experiment sperm were collected 35 days after testicular exposure. Measurements on sperm collected less than three weeks after exposure show no response, indicating the DNA content errors occur before or during meiosis. Sperm collected 10 weeks or more after exposure also showed no increase in CV_D^2. Measurements with a variety of staining protocols and two types of flow cytometers were compared to be certain that artifacts due to the difficulties of sperm measurement were adequately overcome.

The dose response curve is well described by the equation

$$CV_D^2 = BX + CX^2 \qquad (3)$$

where X is the dose in rad. The coefficients B and C found by fitting the data are $B \leq 0.23 \times 10^{-2}$, $C = (0.44 \pm 0.06) \times 10^{-4}$. Note that the slope of the curve is small at low doses and may even be zero. Thus this technique is not sensitive to detecting low radiation exposures. As shown below, this is consistent with other estimates of radiation induced aneuploidy in sperm. Modeling of the shapes of the fluorescence distributions indicates that errors equivalent in magnitude to two whole chromosomes occur at the higher doses and that by 600 rad 30 to 40% of the sperm have abnormal DNA content. Exposure to benzo(a)pyrene and mitomycin-C (MMC) show no increase of CV_D^2 up to lethal doses. The MMC result is consistent with fetal karyotype determinations (6).

Assuming that at low doses the DNA content errors result from single chromosome nondisjunction, that the response is linear with dose, and that the probability of nondisjunction is the same for each chromosome, these measurements allow putting an upper bound on the aneuploidy induction rate in sperm which reach maturity. Due to cell death during spermiogenesis this should be smaller than or equal to the probability of nondisjunction determined immediately after meiosis (sperm count was reduced about 30% by a 100 rad exposure). For single nondisjunction, $CV_D^2 = fCV_A^2$ where f is the fraction of aneuploid sperm and CV_A^2 is the square of the coefficient

of variation of the DNA distribution of all sperm with a single chromosome aneuploidy. For the assumed linear response,

$$f = 2\bar{p} \times N \tag{4}$$

where X is the dose in rads, N is the haploid number of chromosomes and $\bar{p}$ is the probability of a nondisjunction per chromosome per rad in sperm which reach maturity. Using the linear term of equation 3,

$$CV_D^2 = 2\bar{p} \times N\, CV_A^2 \leq 0.23 \times 10^{-2} \times. \tag{5}$$

For the mouse N = 20 and $CV_A^2 = 27$ in units where CV is specified in percent (Table 1). Thus $\bar{p} \leq 0.2 \times 10^{-5}$.

For comparison we can calculate meiotic nondisjunction probabilities from cytological measurements and postfertilization probabilities from analysis of early embryos. Again assuming a linear response, the fraction of aneuploid cells f is given by

$$f = 2pNX \tag{6}$$

where p is the probability of nondisjunction per chromosome per rad, N is the haploid number of chromosomes, and X is the dose in rads. From the data of Szemere and Chandley (22), $p \sim 10^{-5}$ for meiotic metaphase II at 100 rad in the mouse; and from Tates et al. (23,25) $0.25 \times 10^{-5} \leq p \leq 10^{-5}$ for the sex chromosomes in spermatids of the vole M. oeconomous at 100 rads. The frequency of aneuploidy in early mouse embryos whose fathers were exposed to

x rays and mitomycin-C was barely measureable (6). For the radiation exposure $p \lesssim 10^{-6}$. Thus the flow cytometric results are consistent with other determinations of the nondisjunction rate. The fact that the sensitivity of all these detection methods is low is fundamentally due to the low probability of radiation induced nondisjunction. Cytological methods, which allow direct visualization of the chromosomes and individual counting of the errors, have the greatest potential sensitivity but require high effort.

The above comparison has been predicated on the assumption that the DNA content errors are due to whole chromosome aneuploidies. The flow cytometric results shed no light on this assumption since all that is measured is the total sperm DNA content. Cytologic data (22) indicates that at doses up to 200 rad single chromosome aneuploidy occurs, while at higher doses a more complex fragmentation of the genome may dominate. I have also assumed a linear response up to 100 rad in extracting the values of p from the cytologic data. The flow measurements indicate that by 100 rad the response is dominated by the quadratic term (the C coefficient of Eq. (3) even assuming the maximum value for the linear term. Given the experimental uncertainties both in the cytologic and flow data a more rigorous comparison is not warranted. The one presented above serves to demonstrate the rough agreement of the results.

3.3 Comparative Sensitivity of Animal Systems

The relative ability to detect sperm with abnormal DNA content in different species depends both on the aneuploidy probability and the spectrum of the DNA content errors. In the model calculations performed above, this depends on $\bar{p}$ and the distribution of chromosome sizes, CV_A^2. Applying Eq. (6), $CV_D^2 = 2\ \bar{p}\ N\ X\ CV_A^2$. In Fig. 9 the DNA content distributions

of normal sperm and those with a single chromosome error are shown for the mouse, Microtus montanus, and Microtus oregoni. The separation of the X and Y sperm peaks, N, CV_A^2 and N CV_A^2 are shown for these as well as the human in Table 1. Note that if the value of $\bar{p}$ is comparable for all of these species, detection of aneuploidy in the human should be as sensitive as in the mouse, while the two types of Microtus may offer a doubling or tripling of the sensitivity. M. montanus is attractive because the smaller split between the X and Y populations of normal sperm may make it easier to detect cells with slightly abnormal DNA content. An ideal species would have X and Y chromosomes of equal size.

The distributions of Fig. 9 suggest an alternative detection strategy. Rather than trying to measure all aneuploid sperm, one could just detect those containing errors of the larger chromosomes. For example, both M. montanus and M. oregoni contain 8 or 9 errors that would result (if they are compatible with cell survival) in sperm departing by 10% or more from the mean DNA content. Thus one would expect, using $\bar{p} = 10^{-6}$, a frequency of about 10^{-5} per rad for aneuploid sperm with large DNA content errors. The rarity of these events makes their detection difficult in the face of the normally expected fluorescent debris. Measurements of the debris frequency present in bull sperm samples indicate that a sensitivity of a few tens of rads might be possible if the assumption of $\bar{p} \sim 10^{-6}$ is correct. Sorting of these suspected aneuploid sperm for a confirmatory analysis would be required, at least until confidence in the procedure was established.

4. CONCLUSION

Both image analysis and slit-scan flow cytometry have the ability to detect head shape abnormalities in sperm. Their eventual application is

unclear since results to date have been restricted by training sets of data. In the current state of development, a specifically tailored set of shape parameters in conjunction with computer image processing promises the most sensitivity.

The incidence of diploid sperm may be a sensitive biological dosimeter for x rays but uncertainties in the low dose region of the response curve need to be resolved. Measurement of total DNA content can detect induced aneuploidy in sperm. However, the sensitivity to x ray exposure is low because of the small size and low frequency of the DNA content errors.

5. REFERENCES

1. Beaty RA, Fechheimer NS (1972) Diploid spermatozoa in rabbit semen and their experimental separation from haploid spermatozoa. Bio of Reprod 7:267-277

2. Benaron DA, Gray JW, Gledhill BL, Lake S, Wyrobek AJ, Young IT (1982) Quantification of mammalian sperm morphology by slit-scan flow cytometry. Cytometry 2:344-349

3. Brandriff B, Gordon L, Watchmaker G, Ashworth L, Carrano A, Wyrobek AJ (1982) Analysis of sperm chromosomes in normal healthy men using the human-sperm/hamster-egg in vitro fertilization system. Abstracts Amer Soc Human Genet 33rd Ann Mtg, Detroit, Mich., Sept. 29-Oct. 2, 1982

4. Brandriff B, Gordon L, Carrano AV, Ashworth L, Watchmaker G, Wyrobek AJ (1983) Direct analysis of human sperm chromosomes: comparison among four individuals (in preparation)

5. Bruce WR, Furrer R, Wyrobek AJ (1974) Abnormalities in the shape of murine sperm after acute testicular x-irradiation. Mutat Res 23:381-386

6. Chandley AC, Speed RM (1979) Testing for nondisjunction in the mouse. Environ Health Perspect 31:123-124

7. Fraser LR, Mandlin I (1979) Analysis of aneuploidy in first-cleavage mouse embryos fertilized in vitro and in vivo. Environ Health Perspect 31:141-149

8. Garner DL, Gledhill BL, Pinkel D, Lake S, Stephenson D, Van Dilla MA, Johnson LA (1983) Quantification of the X- and Y-chromosome-bearing spermatozoa of domestic animals by flow cytometry. Biol Reprod 28:312-321

9. Gledhill BL (1964) Cytophotometry of presumed diploid bull spermatozoa. Nord Vet-Med 17:328-335

10. Hacker U (1983) . . . . . This volume.

11. Hacker U, Schumann J, Göhde W, Müller K (1981) Mammalian spermatogenesis as a biological dosimeter for radiation. Acta Radiol Oncology 20:279-282

12. Hansmann I, Probeck HD (1979) Detection of nondisjunction in mammals. Environ Health Perspect 31:161-165

13. Illisson L (1969) Spermatozoal head dimensions in two inbred strains of mice and their F_1 and F_2 progenies. Australian J Biol Sci 22:947-963

14. Martin RH, Lin CC, Balkan W, Burns K (1982) Direct chromosomal analysis of human spermatozoa: preliminary results from 18 normal men. Am J Hum Genet 34:459-468

15. Meistrich ML, Göhde W, White RA (1978) Resolution of X and Y spermatids by pulse cytophotometry. Nature 274:821-823

16. Moore II DH, Bennett DH, Kranzler D, Wyrobek AJ (1982) Quantitative methods of measuring the sensitivity of the mouse sperm morphology assay. Analyt and Quant Cytol 4:199-206

17. Otto FJ, Hacker U, Zante J, Schumann J, Göhde W, Meistrich ML (1979) Flow cytometry of human spermatozoa. Histochemistry 62:249-254

18. Pinkel D, Gledhill BL, Lake S, Stephenson D, Van Dilla MA (1982) Sex preselection in mammals? Separation of sperm bearing Y and "O" chromosomes in the vole Microtus oregoni. Science 218:904-906

19. Pinkel D, Gledhill BL, Van Dilla MA, Lake S, Wyrobek AJ (1983) Radiation-induced DNA content variability in mouse sperm. Radiat Res (in press)

20. Pinkel D, Lake S, Gledhill BL, Van Dilla MA, Stephenson D, Watchmaker G (1982) High resolution DNA content measurements of mammalian sperm. Cytometry 3:1-9

21. Searle AG, Beechey CV, Green D, Humphreys ER (1976) Cytogenetic effects of protracted exposures to alpha-particles from plutonium-239 and to gamma-rays from cobalt-60 compared in male mice. Mutat Res 41:297-310

22. Szmere G, Chandley AC (1975) Trisomy and triploidy induced by x-irradiation of mouse spermatocytes. Mutat Res 33:229-238

23. Tates AD (1979) Microtus oeconomus (Rodentia), a useful mammal for studying the induction of sex-chromosome nondisjunction and diploid gametes in male sperm cells. Environ Health Perspect 31:151-159

24. Tates AD, Pearson PL, Geraedts JPM (1975) Identification of X and Y spermatozoa in the northern vole Microtus oeconomus. J Reprod Fertil 42:195-198

25. Tates AD, Pearson PL, Ploeg Mvd, de Vogel N (1979) The induction of sex-chromosomal nondisjunction and diploid spermatids following x-irradiation of pre-spermatid stages in the northern vole Microtus oeconomus. Mutat Res 61:87-101

26. Van Dilla MA, Gledhill BL, Lake S, Dean PN, Gray JW, Kacher V, Barlogie B, Göhde W (1977) Measurement of mammalian sperm deoxyribonucleic acid by flow cytometry - problems and approaches. J Histochem Cytochem 25:763-773

27. Wyrobek AJ, Bruce WR (1978) The induction of sperm shape abnormalities in mice and humans. In: Hollaender A, de Serres F (eds) Chemical mutagens, Vol 5. Plenum Publishing Corp, New York, p. 257

28. Wyrobek AJ, Gordon LA, Burkhart JG, Francis MW, Kapp RW, Letz G, Malling HV, Topham JC, Whorton MD (1983) An evaluation of the mouse sperm morphology test and other sperm tests in nonhuman mammals. Mutat Res 115:1-72

29. Wyrobek AJ, Gordon LA, Burkhart JG, Francis MW, Kapp RW, Letz G, Malling HV, Topham JC, Whorton MD (1983) An evaluation of human sperm as indicators of chemically induced alterations of spermatogenic function. Mutat Res 115:73-148

30. Young IT, Gledhill BL, Lake S, Wyrobek AJ (1982) Quantitative analysis of radiation induced changes in sperm morphology. Analyt and Quant Cytol 4:297-216

Table 1

Comparison of Factors Related to Dose Response Sensitivity

	ΔXY[(a)]	CV_A^2 [(b)]	N[(c)]	NCV_A^2[(d)]
Human	3.0	24	23	552
Mouse	3.2	27	20	540
Microtus montanus	2.5	100	12	1200
Microtus oregoni	9.2	180	9	1620

(a) DNA content difference of X- and Y-chromosome bearing sperm, percent.

(b) Square of coefficient of variation of DNA distribution of sperm with all possible single chromosome aneuploidies. Probability is assumed equal for each chromosome. The number encompases both X and Y subpopulations. Units are percent squared.

(c) Haploid number of chromosomes.

(d) Expected dose response given by Eq. (5) is $CV_D^2 = 2\ \bar{p}\ X\ NCV_A^2$, where $\bar{p}$ is the probability of nondisjunction per chromosome per rad and X is the dose in rads.

FIGURE LEGENDS

Figure 1 Definition of measurements used to describe shape of mouse sperm heads (16). The indicated measurements were manually obtained on enlarged photographs of the sperm heads. In addition to the measurements shown, perimeter, area, and shape factor were also determined.

Figure 2 Sperm head outlines obtained by an automated image analysis system (30).

Figure 3 Dose response curve as a function of the critical value of M (16). Sperm heads with M greater than the critical value were classified as abnormally shaped.

Figure 4 Sperm morphology measurement by slit scan flow cytometry (2). Fluorescently stained sperm heads flow lengthwise through an elliptically focused laser beam. The time course of the signal intensity gives the distribution of dye along the sperm head and thus an indication of head shape.

Figure 5 Comparison of the percent abnormal sperm classified by slit-scan flow cytometry and by a trained visual observer. The SSD threshold has been chosen to maximize the slope at the expense of classifying a larger number of sperm from unexposed animals as atypical (2).

Figure 6 Accurate DNA content measurements of mammalian sperm require special techniques.

a) The high index of refraction causes fluorescence to be preferentially emitted in the plane of these flat cells. The measured brightness thus depends on the cell orientation during

measurement. Randomly oriented sperm yield a distribution as shown when a flow cytometer with the flow axis orthogonal to the optical axis of the detector is used.

b) Hydrodynamic orientation of the sperm allows accurate measurements. Sperm are oriented so they are illuminated on one flat face and fluorescence is collected from the other.

c) Good measurements are also obtained in a system where the cells flow along the optical axis of the cytometer. The rotational symmetry of this geometry makes it insensitive to variations in cell orientation.

Figure 7 Incidence of diploid sperm as a function of radiation dose. The three species shown have about the same background incidence. Microtus data is from Reference 23. Mouse and human data are preliminary.

Figure 8 Increased DNA content variability as a function of radiation dose. The square of the dose dependent part of the coefficient of variation, CV_D^2, is shown as a function of radiation exposure as determined by several combinations of staining and flow cytometric techniques: Solid circles -- acriflavine-Feulgen stain and orienting flow cytometer. Squares -- ethidium bromide-mithramycin double stain and orienting flow cytometer. Open circles 4-6 diamidino-2-phenylindole (DAPI) stain and ICP22 flow cytometer. The solid line is a fit of an equation of the form $CV_D^2 = BX + CX^2$ where X is the dose and B and C are coefficients whose values are given in the text.

Figure 9. The DNA distributions of normal sperm (line) and sperm with single chromosome aneuploidies (solid area) in sperm from three species. The distributions for the normal are shown broadened as they appear in flow cytometric histograms. ΔXY is the percentage DNA content difference between X and Y sperm. In M. oregoni ΔXY refers to the difference between the Y and "O" sperm populations (18).

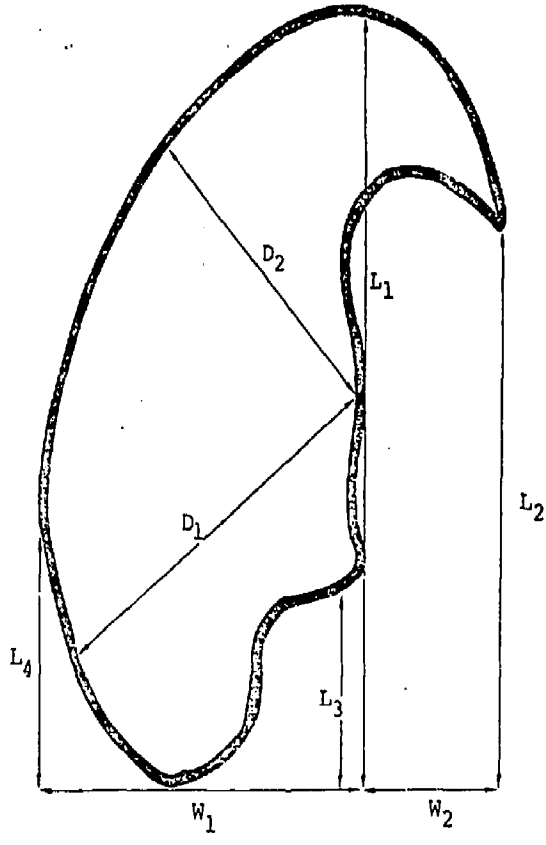

Figure 1

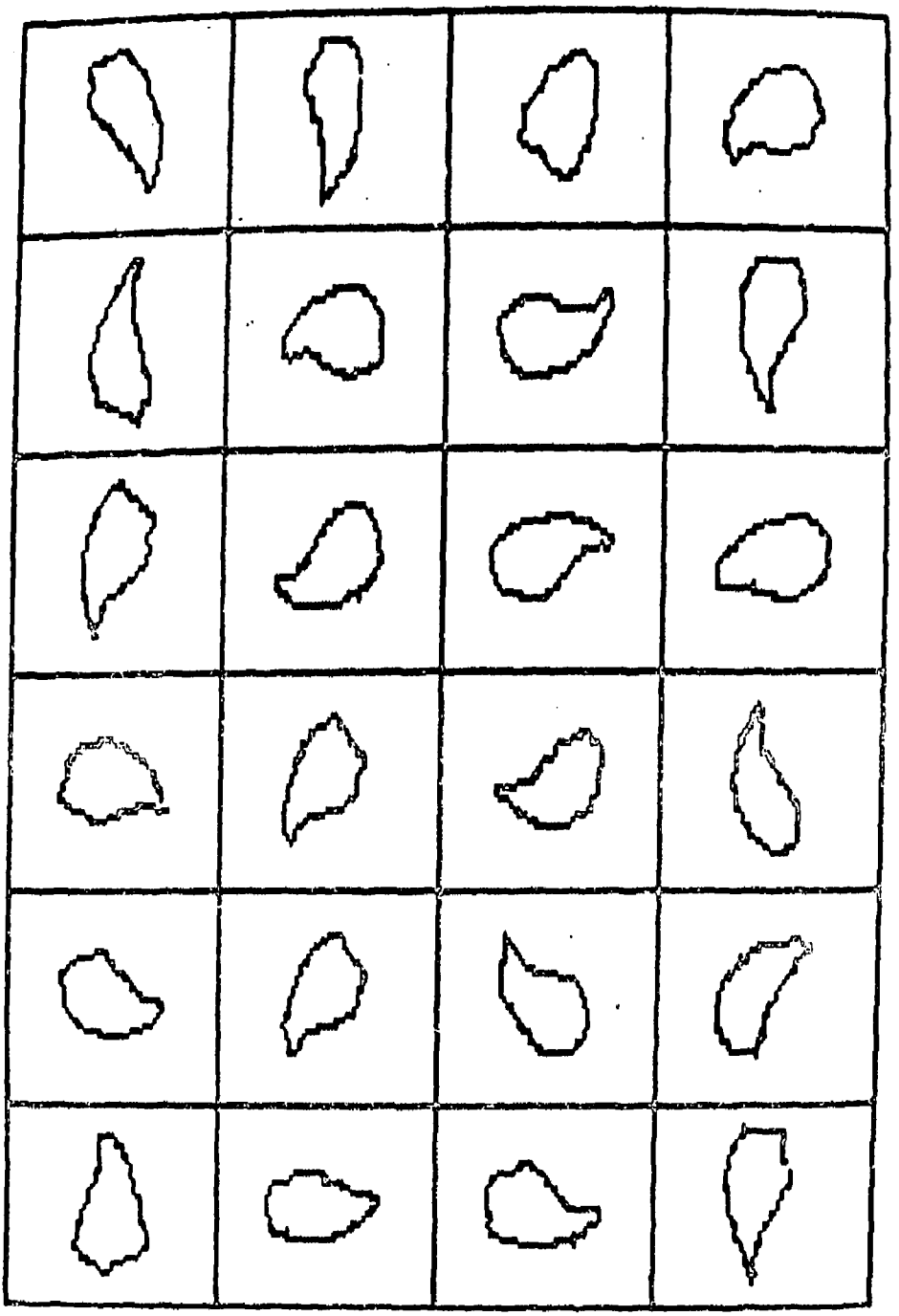

Figure 2

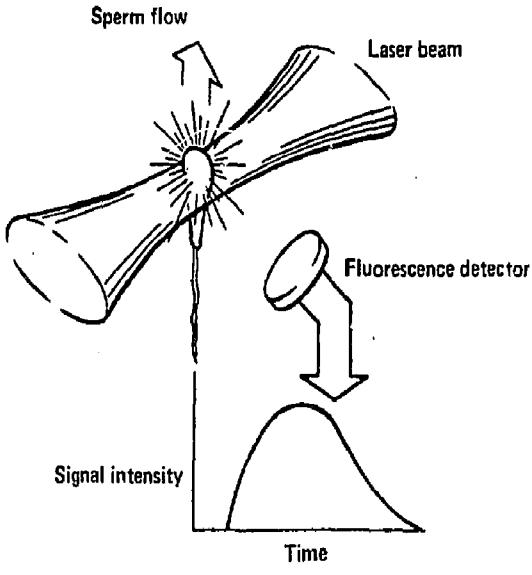
Sperm flow
Laser beam
Fluorescence detector
Signal intensity
Time

Figure 3

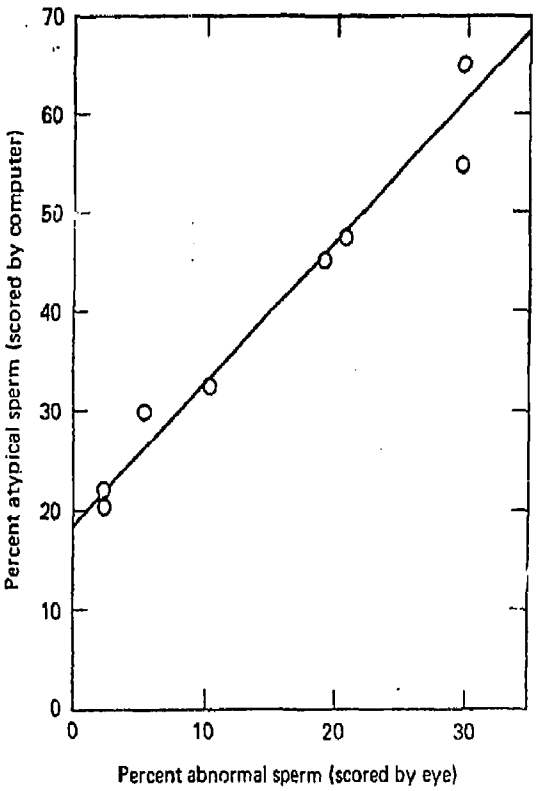
70
60
50
40
30
20
10
0
0
10
20
30
Percent atypical sperm (scored by computer)
Percent abnormal sperm (scored by eye)

Figure 4

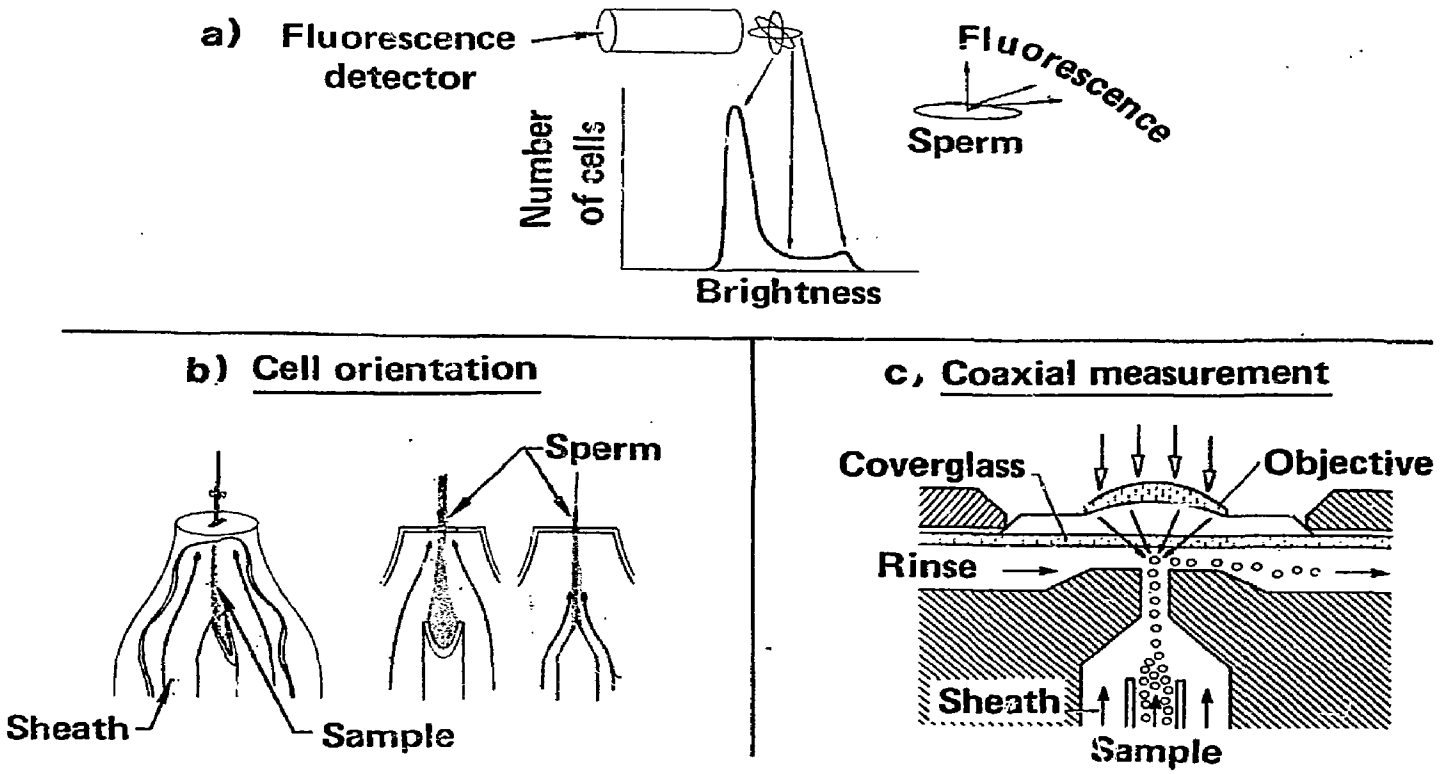
a) Fluorescence detector
Number of cells
Brightness
Fluorescence
Sperm
b) Cell orientation
Sperm
Sheath
Sample
c, Coaxial measurement
Coverglass
Objective
Rinse
Sheath
Sample

Figure 5

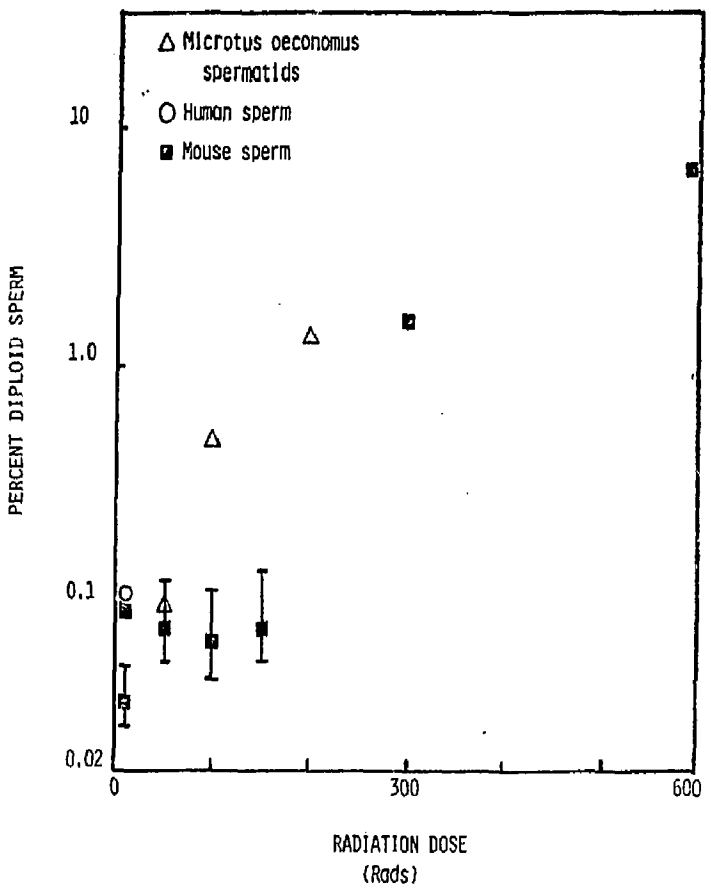
Δ Microtus oeconomus spermatids
O Human sperm
■ Mouse sperm
10
1.0
0.1
0.02
PERCENT DIPLOID SPERM
0
300
600
RADIATION DOSE
(Rads)

Figure 6

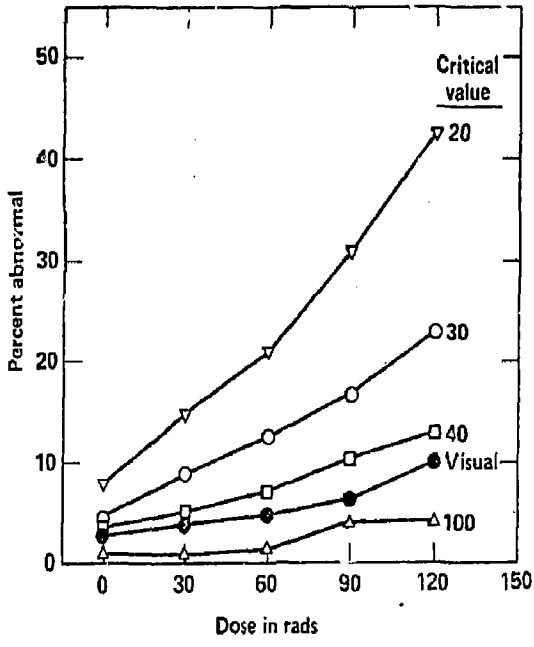
Critical value
20
30
40
Visual
100
Percent abnormal
0
10
20
30
40
50
0
30
60
90
120
150
Dose in rads

Figure 7

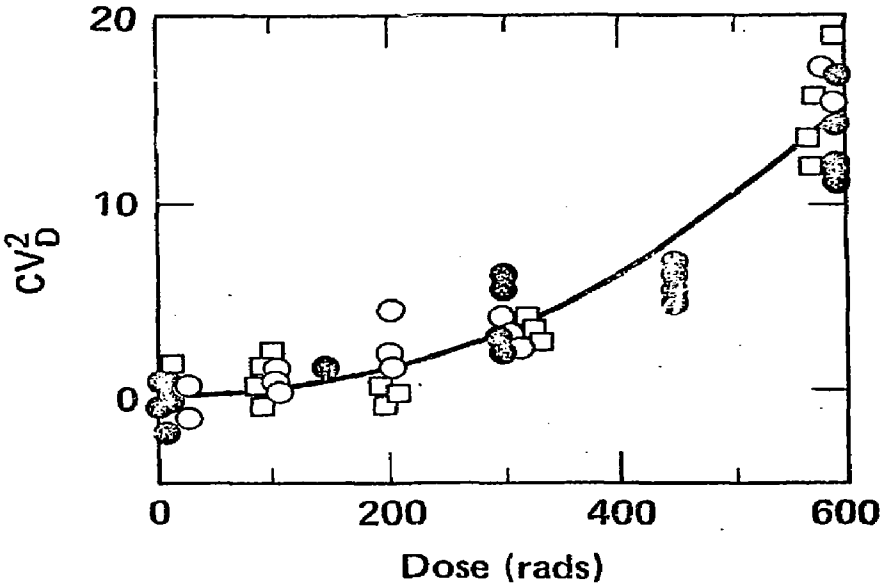

Figure 8

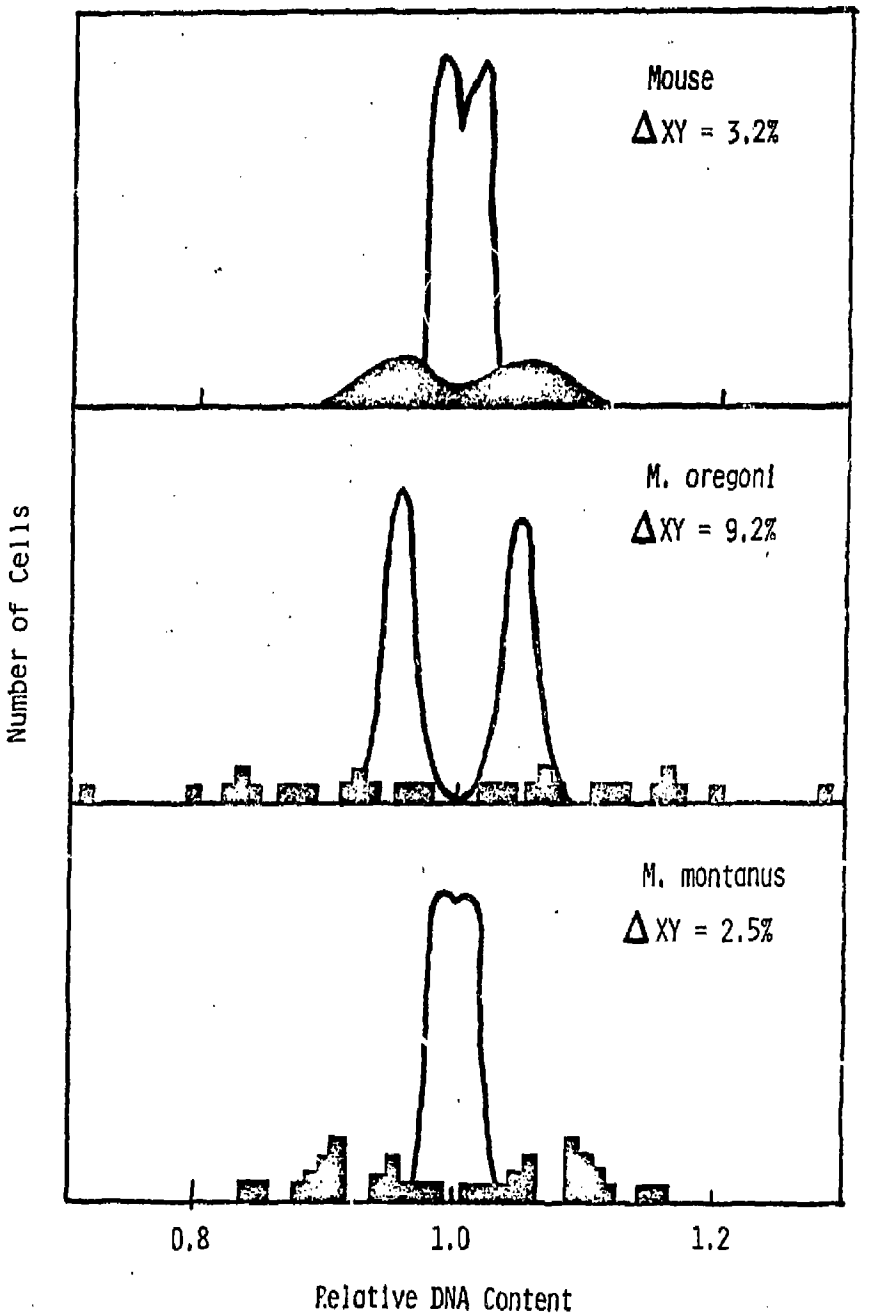
Mouse
ΔXY = 3.2%
M. oregoni
ΔXY = 9.2%
M. montanus
ΔXY = 2.5%
Number of Cells
0.8
1.0
1.2
Relative DNA Content

Figure 9

DISCLAIMER

Technical Information Department · Lawrence Livermore Laboratory
University of California · Livermore, California 94550